Static and thermodynamic properties of liquid and amorphous Fe_2O_3 nanoparticles

2009 J. Phys.: Condens. Matter 21 075103

(http://iopscience.iop.org/0953-8984/21/7/075103)

J. Phys.: Condens. Matter **21** (2009) 075103 (9pp) doi:10.1088/0953-8984/21/7/075103

Static and thermodynamic properties of liquid and amorphous Fe_2O_3 nanoparticles

Vo Van Hoang[1] **and B T H L Khanh**[2]

[1] Department of Physics, Institute of Technology, HoChiMinh City National University, 268 Ly Thuong Kiet Street, District 10, HoChiMinh City, Vietnam
[2] Computational Physics Laboratory, Department of Physics, College of Natural Science, HoChiMinh City National University, 227 Nguyen Van Cu Street, District 5, HoChiMinh City, Vietnam

E-mail: vvhoang2002@yahoo.com

Received 11 October 2008, in final form 22 November 2008
Published 13 January 2009
Online at stacks.iop.org/JPhysCM/21/075103

Abstract
Molecular dynamics (MD) simulation of the structure and thermodynamic properties of liquid and amorphous Fe_2O_3 nanoparticles, with different sizes ranging from 2 to 5 nm, has been carried out based on the Born–Mayer pair potentials under non-periodic boundary conditions. The partial radial distribution functions (PRDFs), coordination number distributions, bond-angle distributions and interatomic distances of liquid nanoparticles at 3500 K were calculated in detail. In addition, we show the radial density profile and stoichiometry in nanoparticles. The temperature dependence of the surface structure and surface energy of nanoparticles has been obtained and presented. Moreover, the size dependence of the glass transition temperature has been found and discussed.

1. Introduction

Fe_2O_3 nanoparticles with a diameter ranging from 1 to 25 nm have been the subject of both experiments and computer simulations in recent years [1–7]. There has been great scientific interest in the synthesis of Fe_2O_3 nanoparticles and in modifications of their size, morphology and properties for different applications [8–14]. For instance, magnetic iron oxide nanoparticles can be widely used as magnetic pigments in recording and information-storage media, catalysis, magnetic fluids, magneto-optical devices and studies of macroscopic quantum tunneling [15–19]. The structure of Fe_2O_3 nanoparticles of different sizes has been investigated using the extended x-ray absorption fine-structure technique (EXAFS) [3], the x-ray absorption near-edge structure (XANES) [4] and the techniques of TEM, XRD and AFM [20]. These studies not only revealed the existence of undercoordinated Fe sites in the nanoparticles but also showed the interplay between surface effects and the peculiar properties of the nanoparticles. Additionally, surface effects in the Fe_2O_3 nanoparticles are more pronounced as the particle size decreases [2, 6, 21]. On the other hand, more detailed information of the structure and properties of Fe_2O_3 nanoparticles at the atomistic level can be provided by computer simulation. However, much attention has been paid to the simulation of the effects of surface and size on the magnetic properties of γ-Fe_2O_3 [6, 7]. Recently, we found size effects on the structure of amorphous Fe_2O_3 nanoparticles via molecular dynamics (MD) simulation [22]. However, no comprehensive work related to the simulation of static and thermodynamic properties of liquid and amorphous Fe_2O_3 nanoparticles has been found in literature yet. This motivated us to carry out a study in this direction.

In this paper we probe the microstructure and thermodynamics of liquid and amorphous Fe_2O_3 nanoparticles by using MD simulation. Size effects on the properties of the surface shell of liquid nanoparticles at 3500 K have been analyzed in detail and compared with that observed in the core and in the bulk counterpart. In order to provide more detailed information about the structure and thermodynamics of the nanoparticles, we present the results of temperature dependence of surface energy and stoichiometry, as well as the size dependence of the glass transition temperature.

2. Calculation

We carried out the simulations in a spherical model with different diameters of 2, 3, 4 and 5 nm containing 410, 1385, 3280 and 6405 atoms, respectively. Each model contains the

Table 1. Structural characteristics of liquid Fe_2O_3 at 3500 K; r_{ij} is the position of the first peaks in PRDFs; θ_{ijk} is the main peak in bond-angle distribution; Z_{ij} is the average coordination number.

	r_{ij} (Å)			θ_{ijk} (deg)		Z_{ij}			
Materials	Fe–Fe	Fe–O	O–O	Fe–O–Fe	O–Fe–O	Fe–Fe	Fe–O	O–Fe	O–O
2 nm	3.10	1.90	2.70	101.75	81.15	9.02	4.71	3.14	7.65
3 nm	3.10	1.90	2.70	99.23	81.86	10.21	5.00	3.34	8.55
4 nm	3.10	1.90	2.70	98.34	83.63	10.81	5.17	3.44	9.21
5 nm	3.10	1.90	2.70	98.05	85.76	11.20	5.28	3.53	9.61
Bulk	3.10	1.90	2.70	97.16	80.45	11.57	5.32	3.55	9.88
Exp. for bulk [24]	3.35	1.91–1.95	2.91			13.50	5.25	4.00	12.00
Exp. for bulk [3]		1.925–1.945							

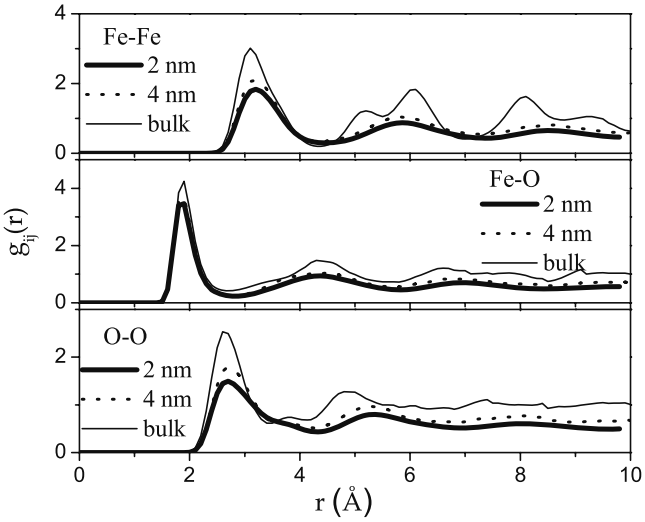

Figure 1. Partial radial distribution functions in liquid Fe_2O_3 nanoparticles at 3500 K compared with those observed in the bulk model at the same temperature.

number of Fe and O atoms in accordance with the Fe_2O_3 stoichiometry. We use an interatomic potential of the Born–Mayer type which was used successfully for models of non-crystalline Fe_2O_3 at 0 and 2000 K [23]. The potential has the following form:

$$U_{ij}(r) = \frac{q_i q_j}{r} + B_{ij} \exp\left(-\frac{r}{R_{ij}}\right) \qquad (1)$$

where the terms represent Coulomb and repulsion energies, respectively. Parameter r is the distance between the centers of ions i and j; $q_i and q_j$ are the charges of ith and jth ions; $q_{Fe} = +3e$, $q_O = -2e$. B_{ij} and R_{ij} are parameters accounting for the repulsion of the ionic shells; $B_{Fe-Fe} = 0$ eV, $B_{Fe-O} = 2453$ eV, $B_{O-O} = 1500$ eV and $R_{ij} = 29$ pm. For the MD method, we used the Verlet algorithm and the MD time step is 1.6 fs. We first placed N atoms randomly in a sphere of fixed radius, and the equilibrated melt at 7000 K was obtained by relaxing for 50 000 MD steps under non-periodic boundary conditions. The system was cooling down from the melt at constant volume corresponding to a system density of 5.19 g cm^{-3}. The temperature of the system was decreased linearly in time as $T = T_0 - \gamma t$ at a cooling rate of $\gamma = 4.357 \times 10^{13}$ K s^{-1}. The amorphous model was obtained at 350 K. Configurations at finite temperatures were relaxed for 50 000 MD steps before calculating static properties. In order to calculate the coordination number and bond-angle distributions in liquid and amorphous Fe_2O_3 nanoparticles, we adopted fixed cutoff radii $R_{Fe-Fe} = 4.30$ Å, $R_{Fe-O} = 2.60$ Å, $R_{O-O} = 3.50$ Å. These values were chosen as the position of the minimum after the first peak in the partial radial distribution functions (PRDFs) for the amorphous bulk at 350 K. The results have been averaged over ten, six and four independent runs for nanoparticles with the size of 2, 3 and 4 nm, respectively. Due to large number of atoms in the model with a size of 5 nm (i.e. 6405 atoms) a single run was done for this size. In order to compare, we also show the results of liquid and amorphous Fe_2O_3 models containing 3000 atoms under periodic boundary conditions which were considered as the bulk counterparts. Note that the bulk models have been obtained by the same cooling procedure at constant volume corresponding to a system density of 5.19 g cm^{-3} like that used for nanoparticles.

3. Results and discussions

3.1. Structure of liquid Fe_2O_3 nanoparticles at 3500 K

In order to study the structural properties of liquid Fe_2O_3 nanoparticles obtained at 3500 K, we start by analyzing the PRDFs for different atomic pairs. As shown in figure 1 and table 1, the interatomic distance for Fe–Fe, Fe–O and O–O in nanoparticles is found to be similar to those for the bulk. It has slightly smaller value compared with those observed in practice for the bulk [3, 24]. On the other hand, we found no splitting of the first peak in the PRDFs for the Fe–Fe pair in nanoparticles unlike that observed in the amorphous one [22], i.e. the first peak is centered at around 3.11 Å and the second one is at 3.40 Å [22]. As discussed in [22], the shorter Fe–Fe bond length of 3.11 Å is related to the pairs of octahedral Fe sites linked by their edge, the longer one of 3.40 Å is for pairs of octahedral Fe sites having a common vertex. In addition, we compared the results for four particle diameters (2, 3, 4 and 5 nm) with those for the bulk (table 1). The main feature observed is that the mean coordination number for all atomic pairs in nanoparticles increases with their size toward the value for the bulk. The mean coordination number Z_{Fe-O} ranges from 4.71 to 5.28, indicating the tendency to form a distorted octahedral network structure of liquid Fe_2O_3

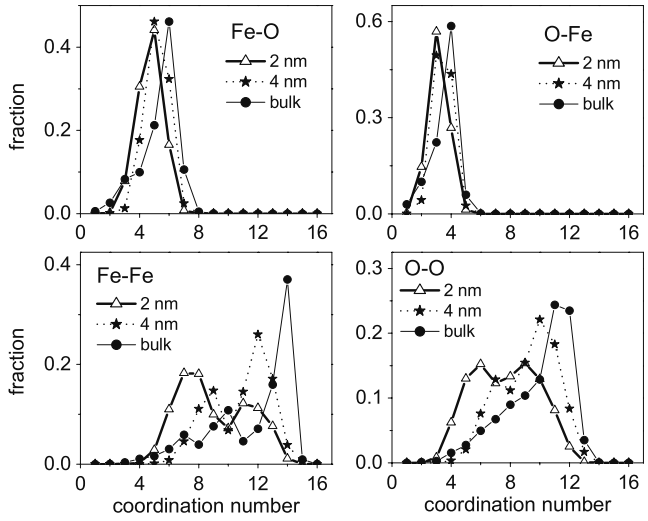

Figure 2. Coordination number distribution in liquid Fe_2O_3 nanoparticles at 3500 K compared with that observed in the bulk model at the same temperature.

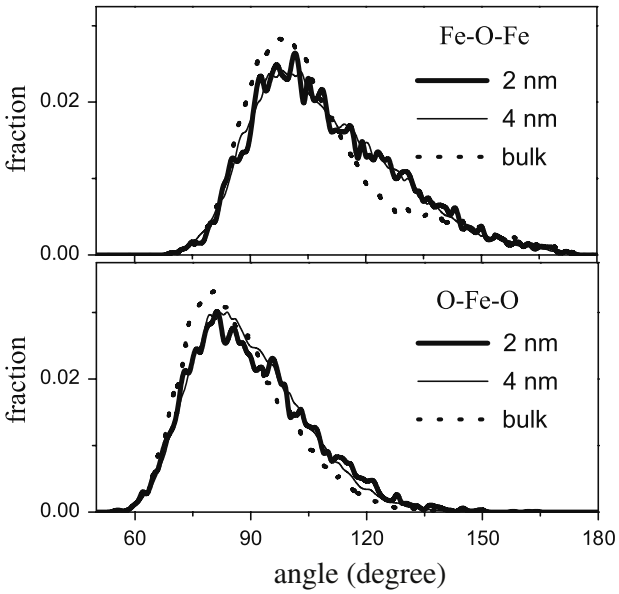

Figure 3. Bond-angle distribution in liquid Fe_2O_3 nanoparticles at 3500 K.

nanoparticles if their size is large enough, like that observed in the bulk [23], and is in accordance with [3, 4, 24]. Due to the reduction of surface effects, structural properties of liquid Fe_2O_3 nanoparticles are closer to those for the bulk as the particle size increases (see table 1).

More detailed information about local structure can be obtained from the coordination number and bond-angle distributions (figures 2 and 3). One can see that the coordination number distributions in nanoparticles are size dependent and they differ from those of the bulk, indicating the presence of surface effects in the systems. For instance, the peaks in the coordination number distributions of nanoparticles were located at the value of 5.00 for Fe–O and at 3.00 for O–Fe while that for the bulk is at 6.00 for Fe–O and at 4.00 for O–Fe (see figure 2). Since the bulk amorphous Fe_2O_3 has a distorted octahedral network structure with a mean coordination number for the Fe–O pair of $Z_{Fe-O} \approx 6$, one can consider structural units with $Z_{Fe-O} \neq 6$ as structural defects in the system [22, 23]. Figure 2 shows that liquid Fe_2O_3 nanoparticles contain a large number of structural defects and pentacoordinated Fe sites dominate in nanoparticles. Moreover, the distributions for Fe–Fe and O–O pairs totally differ from each other; this ensures that intermediate scale order (i.e. the linkage between structural units FeO_n) is more sensitive to the nanoparticle size compared with those of local scale order. Regarding the bond-angles, we show in figure 3 only the most important ones such as Fe–O–Fe and O–Fe–O angles; the first one describes the connectivity between FeO_n units in the system and the second one describes the local order inside them. Unlike the smooth curves for the bulk, one can see the appearance of additional peaks in the curves for nanoparticles which are more pronounced for the smallest size of 2 nm. Small peaks in the bond-angle distributions for Fe_2O_3 nanoparticles may be related to the existence of small member rings on the surface of Fe_2O_3 nanoparticles like those observed and discussed for amorphous SiO_2 nanoscale clusters [25]. Distributions for Fe–O–Fe and O–Fe–O bond-angles in nanoparticles have their main peak at around 99° and 83°, respectively. It is well known that for an ideal octahedron, the O–Fe–O angle is equal to 90°, and for an ideal tetrahedron it is equal to 109.5°. This may be due to the existence of FeO_5 units in large amounts in liquid Fe_2O_3 nanoparticles. As seen in table 1, the main peak of the O–Fe–O angle shifts toward a smaller value with decreasing nanoparticle size, indicating the growth tendency of the structural defects as the particle size decreases.

The surface defects in nanoparticles are also clarified by the radial density profile $\rho(R)$, i.e. the radial local density at the distance R from the center of a nanoparticle. This quantity is an important one for gaining more insight into the local structure of nanoparticles. If the number of atoms belonging to the spherical shell of thickness 0.20 Å formed by two spheres with radii $R - 0.10$ Å and $R + 0.10$ Å is determined one can infer $\rho(R)$. As it was done in [26], we calculate $\rho(R)$ directly for radii just beyond a large enough finite value, which is taken equal to 10.00 Å in the present work. The density profile has been averaged over four different configurations, and R increases from 10.00 Å with a step of 0.20 Å. As shown in figure 4, we can see that the total density fluctuates around the value 5.00 g cm^{-3}, which is in qualitative agreement with the density obtained by both experiments and calculations [28]. Additionally, an interesting feature is observed via the separate partial density profile curve for oxygen (figure 4), i.e. oxygen atoms have a tendency to concentrate at the surface of nanoparticles like those observed at liquid SiO_2 or amorphous Al_2O_3 surfaces [25–27]. For this phenomenon, it has been said that the system is energetically favored with an oxygen atom at the surface, since only one bond has to be broken, if any, whereas if an iron is at the surface several bonds have to be broken [25]. In order to achieve local charge neutrality, Fe atoms have a tendency to concentrate in the shell close to the surface due to an excess

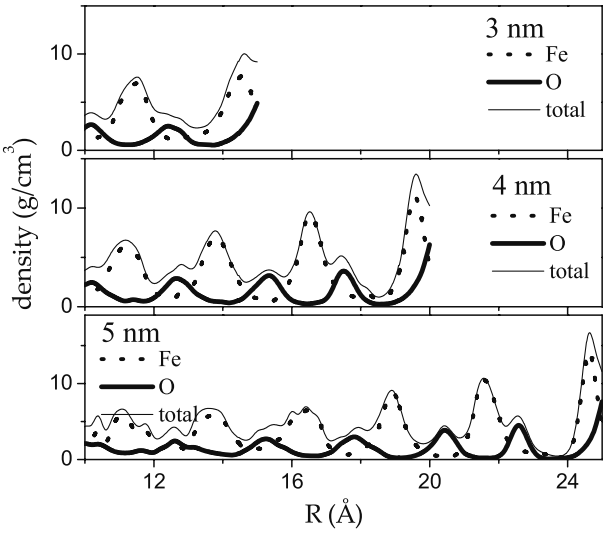

Figure 4. Density profiles in liquid Fe_2O_3 nanoparticles at 3500 K.

of oxygen at the surface [25–27]. This causes the occurrence of a peak of the total density in the vicinity of the surface. Furthermore, Fe and O atoms also have a tendency to both concentrate in the inner shells. This leads to the formation of a so-called layer structure which consists of iron-enriched layers and oxygen-enriched layers (figure 4). For $NiFe_2O_4$ nanoparticles [21], the fraction of surface cations removed at random and the fraction of broken exchange bonds relative to the total number of neighboring pairs of surface cations was calculated to determine the surface vacancy density and the broken bonds density. Surface roughness was created by removing surface cations at random, and the effect of the surface anisotropy became more pronounced when more roughness was added. In particular, the roughness is no longer limited to the outermost monolayer of the initial sphere [21]. Thus, our calculations for the density profiles highlight the situation. On the other hand, the iron-enriched layer was observed by examination of the oxide/Al_6Fe interface in energy-filtering transmission electron microscopy [29]. The fine dark bands, a few nanometers thick, in the transmission electron micrograph was suggested to represent a region of iron enrichment [29–31]. This local character was thought to correlate to the surface heterogeneities [30].

In addition, a similar so-called layer structure has been found for the amorphous SiO_2, GeO_2, TiO_2 nanoparticles [32–34] although the phenomenon is less pronounced for the SiO_2 nanoparticles at the ambient pressure density. The phenomenon is enhanced with increasing density of the system [35, 36]. It may be related to chemical ordering in the binary systems. In contrast, density profiles in the simple monatomic nanoparticles do not show the so-called layer structure, may be because there is only topological ordering in simple monatomic systems [37, 38].

3.2. Surface and core structures of liquid Fe_2O_3 nanoparticles

The surface of nanoparticles has been investigated intensively in recent years because of the important role of the surface in the peculiar properties of nanoparticles. Usually, nanoscale materials are thought to consist of two components, i.e. the core and the surface parts. It is necessary to decide which atoms belong to the surface and which ones belong to the core of nanoparticles. There is no common rule for the choice. For DBS-coated and CTAB-coated Fe_2O_3 nanoparticles, the thicknesses of the surface layers were estimated to be 5.0 Å and 7.0 Å, respectively [3]. For amorphous SiO_2, all atoms that were within 5.0 Å of the hull were defined to belong to the surface; all atoms that were between 5.0 and 8.0 Å from the hull were defined to belong to a transition zone; the remaining atoms were defined to belong to the interior of the droplet [25]. For amorphous Al_2O_3 thin film the top 1.0 or 3.0 Å layer of the amorphous thin film was used for surface structural studies [27]. From a structural point of view it can be considered that atoms belong to the surface if they could not have full coordination for all atomic pairs in principle; in contrast, atoms belong to the core if they can have full coordination for all atomic pairs in principle like those located in the bulk. Therefore, we assume that the atoms located in the outer shell of a Fe_2O_3 spherical nanoparticle with a thickness of 4.29 Å (i.e. the largest radius of the coordination spheres used in the system) belong to the surface and remaining atoms belong to the core of the nanoparticle. A similar rule was used for amorphous nanoparticles of different substances in [32–38]. One can see that our value 4.29 Å for the surface thickness of amorphous Fe_2O_3 nanoparticles is close to that estimated in [3].

Mean coordination numbers for all atomic pairs in the surface shell and in the core of Fe_2O_3 nanoparticles at 3500 K are presented in table 2. One can see that the mean coordination number for all atomic pairs in the surface shell increases with increasing particle size, while in the core it almost remains unchanged. Moreover, structural characteristics of the core of Fe_2O_3 nanoparticles are close to those of the bulk, while the structure of the surface substantially differs from that of the bulk due to the surface defect sites. In addition, the mean coordination number for all atomic pairs in the core of Fe_2O_3 nanoparticles is higher than that of the bulk, indicating the more close-packed structure of the former compared with that of the latter.

The nature of the surface defects of Fe_2O_3 nanoparticles was established as undercoordinated Fe sites with O ligands missing from that of an octahedral coordination. As seen in figure 5, for Fe–O pair coordination number distributions for the surface of liquid Fe_2O_3 nanoparticles at 3500 K have peaks at $Z_{Fe-O} = 5$ compared with $Z_{Fe-O} = 6$ for the bulk, indicating a large number of structural defects in the former due to breaking bonds at the surface. In contrast, the distributions for the core have two peaks at $Z_{Fe-O} = 5$ and 6 for diameters above 4 nm. It has only a peak at $Z_{Fe-O} = 5$ for the small size of 2 nm. Moreover, as shown in table 3, FeO_5 structural units make up the main fraction in the surface shell of liquid Fe_2O_3 nanoparticles, but in the core FeO_5 and FeO_6 units dominate. The fraction of undercoordinated structural units such as FeO_3 and FeO_4 increases with decreasing nanoparticle size in the surface shell due to the surface effects, while in the core the fraction of FeO_6

Table 2. Mean coordination number of the surface and core of liquid Fe_2O_3 nanoparticles at 3500 K.

	Z_{ij} (surface)				Z_{ij} (core)			
Materials	Fe–Fe	Fe–O	O–Fe	O–O	Fe–Fe	Fe–O	O–Fe	O–O
2 nm	8.64	4.63	3.07	7.28	11.55	5.26	3.52	9.50
3 nm	9.51	4.88	3.20	7.98	12.03	5.33	3.60	9.67
4 nm	9.96	5.03	3.28	8.61	12.16	5.38	3.64	9.91
5 nm	10.22	5.16	3.34	9.02	12.30	5.45	3.70	10.12
Bulk	11.57	5.32	3.56	9.88				
Exp. for CTAB-coated [3]		5.20						

Table 3. Coordination number distribution for Fe–O pairs in the surface shell and in the core of Fe_2O_3 nanoparticles at 3500 K. We show the percentage of Fe atoms with a corresponding value of Z_{Fe-O} which ranges from 3 to 7.

	3		4		5		6		7	
Materials	Surface	Core	Surface	Core	Surface	Core	Surface	Core	Surface	Core
2 nm	8.87	0.78	33.37	11.02	43.17	50.39	13.54	37.01	0.81	0.78
3 nm	3.54	0.22	28.18	10.20	46.17	49.13	19.94	37.42	1.87	2.93
4 nm	1.93	0.25	21.88	11.03	48.08	43.08	26.36	41.80	1.55	3.84
5 nm	1.11	0.00	18.90	8.33	44.99	43.78	32.54	42.95	2.45	4.78

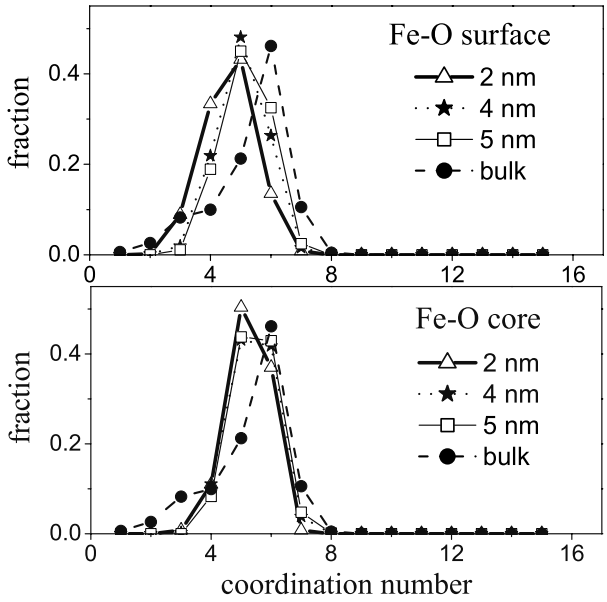

Figure 5. Coordination number distribution for the Fe–O pair in the surface and in the core of liquid Fe_2O_3 nanoparticles at 3500 K.

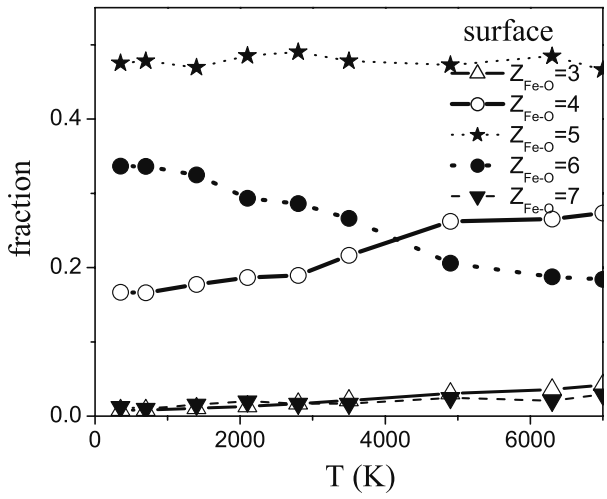

Figure 6. Temperature dependence of the coordination number distribution for the Fe–O pair in the surface shells of 4 nm Fe_2O_3 nanoparticles.

structural units increases as the nanoparticle size increases. The existence of undercoordinated Fe sites on the surface of γ-Fe_2O_3 nanoparticles with diameters of 6.5 and 3.0 nm was studied in detail by Chen *et al* [4]. The ratios of octahedral sites/tetrahedral sites are 83/17 for 6.5 nm nanoparticles and 73/27 for 3.0 nm nanoparticles. The fractions of surface sites are 17 and 26% for nanoparticles with diameters of 6.5 and 3.0 nm, respectively, lower than the calculated surface fractions of 24 and 52% on the basis of the α-Fe_2O_3 lattice structure. This indicates the existence of pentacoordinated square-pyramid geometry in the surface. In addition, the fraction of undercoordinated sites increases with the fraction of surface sites [4]. Similarly, for titanium dioxide (TiO_2) nanoparticles, the distorted octahedral coordination geometry of Ti in the bulk anatase was changed into a pentacoordination geometry on the surface of nanoparticles [4, 39]. Based on the results obtained above one can see that there are a large number of structural defects on the surface of Fe_2O_3 nanoparticles due to the breaking bonds at the surface, like the experimental findings. Structural defects in the surface shell can play an important role in the properties of liquid and amorphous Fe_2O_3 nanoparticles like those found and discussed for SiO_2 and TiO_2 nanoparticles [33, 34].

A temperature dependence of coordination number distribution for the Fe–O pair in the surface shell and in the core of 4 nm Fe_2O_3 nanoparticles is demonstrated in figures 6 and 7. One can see that the percentage of FeO_6 structural units in the core strongly increases with decreasing temperature, while that of the undercoordinated structural units such as FeO_4, FeO_5 decreases. This means that an octahedral network structure becomes the most dominant in the core of Fe_2O_3 nanoparticles

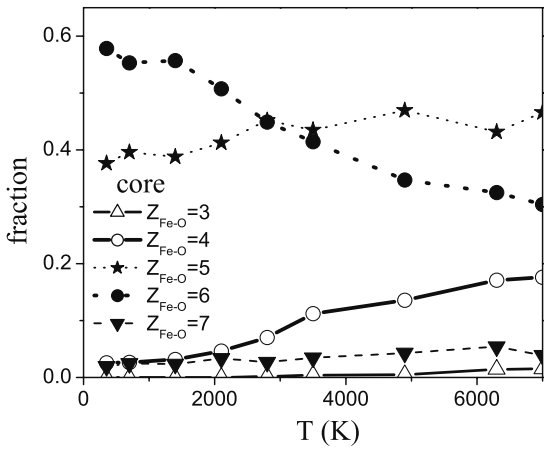

Figure 7. Temperature dependence of the coordination number distribution for the Fe–O pair in the core of 4 nm Fe_2O_3 nanoparticles.

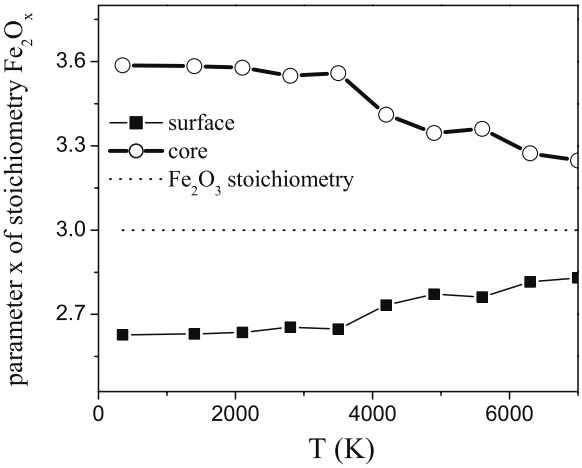

Figure 8. Temperature dependence of Fe_2O_x stoichiometry in the surface shell and in the core of 4 nm Fe_2O_3 nanoparticles.

as the temperature is decreased, i.e. in the amorphous phase at 350 K (see figure 7). In contrast, upon cooling from the melt the percentage of fivefold coordinated Fe atoms to oxygen in the surface shell is relatively unchanged and fluctuates around 48% (see figure 6). We found that the concentration of structural point defects in the surface shell at low temperatures is much higher than that in the core of nanoparticles. In addition, figure 8 shows that the surface has a negative deviation from the Fe_2O_3 stoichiometry, and in contrast the core has a positive deviation for the temperature range studied. This means that oxygen-deficiency defects mainly exist in the surface shell of nanoparticles due to a negative deviation from the Fe_2O_3 stoichiometry. In contrast, oxygen-excess defects mainly exist in the core due to a positive deviation from the Fe_2O_3 stoichiometry. The difference in stoichiometry between the core and the surface shell might be related to the breaking symmetry at the surface [6]. It was found that deviation from perfect stoichiometry and distortion of the position of atoms in the lattice become more important at the surface of the real nanoparticles [40]. On the other hand, the influence of the non-stoichiometry on the magnetic properties has also been elucidated via the core and the surface contributions to the total magnetization [2]. At low temperatures, the core contribution to the magnetization decreases when the nanoparticle diameter diminishes, whereas the surface contribution becomes dominant [2]. Additionally, thermogravimetric analysis and a coulometric titration technique showed that the oxygen stoichiometry of $Sr_{0.97}(Ti, Fe)O_{3-\delta}$ materials varies with temperature [41]. Indeed, temperature dependence of stoichiometry in the core and in the surface shell of Fe_2O_3 nanoparticles was also found in the present work (see figure 8).

3.3. Surface energy and glass transition temperature of liquid Fe_2O_3 nanoparticles

The surface energy (E_s) is one of the quantities used for studying nanoclusters [42], and for testing the validity of different interatomic potentials for describing the surface properties of simulated nanoscale systems [25]. In order to

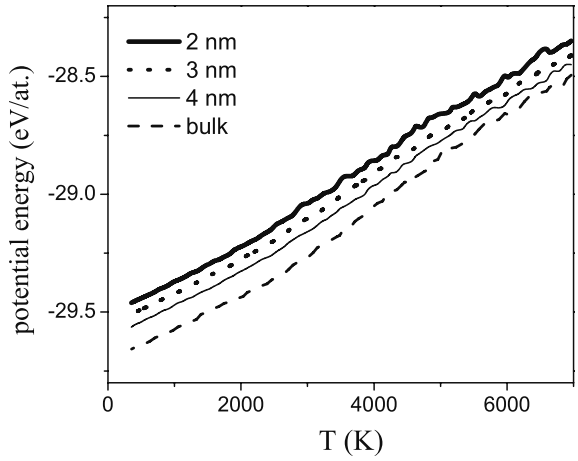

Figure 9. Temperature dependence of the potential energy of Fe_2O_3 nanoparticles.

calculate the surface energy of Fe_2O_3 nanoparticles we first determine the potential energy per atom, E_{pot}. In figure 9, we present the temperature dependence of E_{pot} for Fe_2O_3 nanoparticles of three different diameters compared with that of the bulk. The potential energies decrease as temperature decreases down to 350 K. We see that E_{pot} for the nanoparticles is significantly higher than that for the bulk due to the surface effects, and size effects are clearly observed, i.e. E_{pot} is higher if the particle size is smaller due to the enhancement of the surface effects. Hence, we can assume the relation:

$$E_{pot}^{nano} - E_{pot}^{bulk} = E_s/N \qquad (2)$$

where E_s is the surface energy of the nanoparticle and N is the total number of atoms in the model. We see that in the high temperature region ($T \geqslant 3500$ K) E_s increases with decreasing temperature (figure 10). This is in agreement with experimental findings for the surface tension [43]. In contrast, the value of E_s changes slightly with the temperature range from 350 to 3500 K, i.e. it ranges from about 1.13 to 1.31 J m^{-2} for 3 nm Fe_2O_3 nanoparticles. The energy of reconstructed

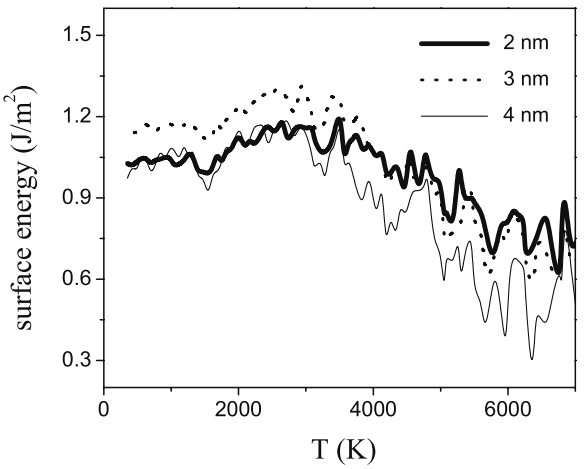

Figure 10. Temperature dependence of the surface energy of Fe_2O_3 nanoparticles.

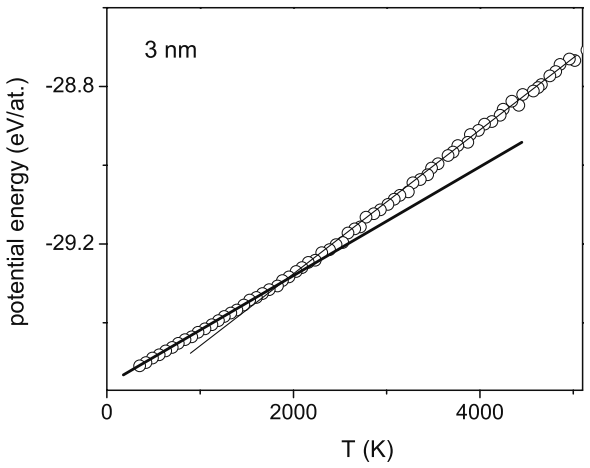

Figure 11. Determination of the glass transition temperature, T_g, of 3 nm Fe_2O_3 nanoparticles.

surfaces of γ-Fe_2O_3 was also calculated, and the calculated surface energy agreed well with those observed experimentally for nanocrystals (with a size of less than 40 nm) [44], i.e. it is around 1.86 J m^{-2} for the surface of γ-Fe_2O_3 containing the (112) surface plane. This means that our calculated value for the surface energy for amorphous Fe_2O_3 nanoparticles is close to the experimental one obtained for γ-Fe_2O_3. On the other hand, the size dependence of the catalytic properties of the compound of Fe_2O_3 nanoparticles can be associated with an influence of size on the electronic structure of the material. This influence may be due to the surface tension of the particle, resulting in changes in the stoichiometry of such particles [45].

In addition, it seems that the temperature dependence of the surface energy of liquid and amorphous Fe_2O_3 nanoparticles has a local peak at around $T = 3000$ K (see figure 10). This may be related to the occurrence of a sudden local change in volume (or density) of the system upon cooling from the melt, like those found for bulk silica using a *NPT* ensemble simulation [46]. Additional oscillations of the curves presented in figure 10 might be related to the poor statistics of the simulation while we averaged the data over only a small number of runs. In contrast, the surface energy of liquid and amorphous SiO_2, TiO_2 and simple monatomic nanoparticles decreases almost monotonically with decreasing temperature [33, 34, 37].

The glass transition temperature is one of the important parameters of amorphous substances. In the present work, the glass transition temperature of Fe_2O_3 nanoparticles, T_g, was found via the intersection of a linear high temperature and low temperature extrapolation of the potential energy of the system as was done for the bulk liquids Al_2O_3–SiO_2 [47] or for TiO_2, SiO_2, $Al_2O_3{\cdot}2SiO_2$ and simple nanoparticles [33, 34, 37, 48] (figure 11). The best estimate of T_g was equal to 2182.18, 1897.26, 1784.19 and 1610.33 K for 2, 3, 4 and 5 nm Fe_2O_3 nanoparticles, respectively. It is clear that T_g is shifted to higher values as the particle size decreases (figure 12) like that found for simulated TiO_2 and simple monatomic nanoparticles [33, 37], and this is in contrast to the values observed experimentally for organic nanoparticles [49] or for

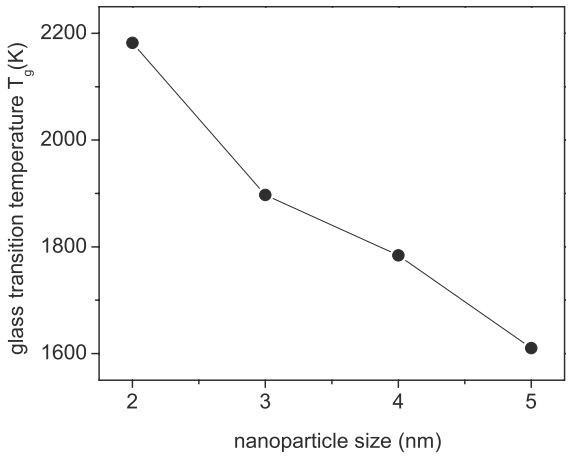

Figure 12. Size dependence of the glass transition temperature, T_g, of liquid Fe_2O_3 nanoparticles.

simulated SiO_2 and $Al_2O_3{\cdot}2SiO_2$ ones [34, 48]. The glass transition temperature for the bulk liquid Fe_2O_3 obtained in the present work has a value of around 1400 K, which is smaller than that for nanoparticles. It is necessary to notice that the error in determining T_g of Fe_2O_3 nanoparticles is smaller than the size of the symbol of the curves presented in figure 12. Generally, the features of a glass transition in liquids are still unclear, including glass transition in nanoscaled systems (i.e. nanoparticles, thin films and those of liquids in confined geometries) which has been under intensive investigations in recent years [49–53]. While the glass transition temperature is typically lower in a confined geometry, experiments have also found cases where T_g increases [54, 55]. The finite size effects on T_g cannot be interpreted as readily as that on the melting temperature T_m due to the lack of a consensus about the nature of the glass transition [56, 57]. Results related to the glass transition at the nanoscale show an increasing, decreasing or no effect depending on the experimental method, the materials studied and the group of researchers (see review in [53] and references therein). Several parameters which may influence the glass transition in

the system at the nanoscale can be considered, such as size effects, interfacial effects, macroscopic confinement effects and boundary conditions [53, 58]. The atomic size σ may be considered as an additional parameter [50].

4. Conclusion

We investigated the structure and thermodynamics of liquid and amorphous Fe_2O_3 nanoparticles in spherical models with different diameters of 2, 3, 4 and 5 nm over a wide temperature range by using MD simulation. Our calculations show that the structure of liquid and amorphous Fe_2O_3 nanoparticles is strongly size dependent in that the mean coordination number for all atomic pairs in nanoparticles increases with their size toward the value for the bulk. A strongly distorted octahedral network structure mainly exists in nanoparticles if their size is large enough. The formation of a so-called layer structure which consists of iron-enriched and oxygen-enriched layers was observed in liquid and amorphous Fe_2O_3 nanoparticles via the radial density profile. The surface structure of Fe_2O_3 nanoparticles is very different from that observed in the core and in the bulk. Undercoordinated structural units such as FeO_4, FeO_5 dominate in the surface shell due to the breaking of bonds at the surfaces. At low temperatures, an octahedral network structure becomes the most dominant in the core of Fe_2O_3 nanoparticles, while fivefold coordinated Fe atoms to oxygen dominate in the surface shell and their fraction is relatively unchanged upon cooling from the melt. In addition, the stoichiometries in the surface shell and in the core are also different from each other, i.e. oxygen-deficiency defects mainly exist in the surface shell. In contrast, so-called oxygen-excess defects mainly exist in the core of Fe_2O_3 nanoparticles. It was found that in the high temperature range ($T \geqslant 3500$ K) the surface energy of Fe_2O_3 nanoparticles increases with decreasing temperature. This is in agreement with experimental findings for the surface tension. However, at lower temperatures it has a tendency to decrease with decreasing temperature. On the other hand, our calculated surface energy for Fe_2O_3 nanoparticles has a value close to that obtained experimentally for γ-Fe_2O_3. The glass transition temperature of liquid Fe_2O_3 nanoparticles is size dependent in that it shifts to higher values as the particle size decreases.

References

[1] Machala L, Zboril R and Gendanken A 2007 *J. Phys. Chem.* B **111** 4003
[2] Mazo-Zuluaga J, Restrepo J and Mejia-Lopez J 2008 *J. Phys.: Condens. Matter* **20** 195213
[3] Zhonghua W, Lin G, Qianshu L and Hesun Z 1999 *J. Phys.: Condens. Matter* **11** 4961
[4] Chen L X, Liu T, Thurnauer M C, Csencsits R and Rajh T 2002 *J. Phys. Chem.* B **106** 8539
[5] Liao X, Zhu J, Zhong W and Chen H Y 2000 *Mater. Lett.* **50** 341
[6] Iglesias O and Labarta A 2001 *Phys. Rev.* B **63** 184416
[7] Kachkachi H, Ezzir A, Nogues M and Tronc E 2000 *Eur. Phys. J.* B **14** 681
[8] Music S, Czako-Nagy I, Salaj-Obelic I and Ljubesic N 1997 *Mater. Lett.* **32** 301
[9] Vollath D, Szabo D V, Taylor R D and Willis J O 1997 *J. Mater. Res.* **12** 2175
[10] Peng J and Chai C C 1993 *Sensors Actuators* B **13/14** 591
[11] Peng Y Q, Wang T, Zou S Y, Bu W and Zheng L D 1994 *Acta Phys. Sin.* **43** 1208
[12] Fei H S, Gao M Y, Ai X C, Yang Y Q, Zhang T Q and Shen J C 1996 *Appl. Phys.* A **62** 525
[13] Bodker F, Morup S and Linderoth S 1994 *Phys. Rev. Lett.* **72** 282
[14] Ai X C, Fei H S and Yang Y Q 1994 *J. Lumin.* **61** + **62** 364
[15] Ensling J, Gutlich P, Klinger R, Meisel W, Jachow H and Schwab H 1998 *Hyperfine Interact.* **111** 143
[16] Teng X W, Black D, Watkins N J, Gao Y L and Yang H 2003 *Nano Lett.* **3** 261
[17] Depeyrot J, Sousa E C, Aquino R, Tourinho F A, Dubois E, Bacri J C and Perzynski R 2000 *J. Magn. Magn. Mater.* **252** 375
[18] Zayat M Z, del Monte F, Morales M D, Rosa G, Guerrero H, Serna C J and Levy D 2003 *Adv. Mater.* **15** 1809
[19] Tejada J, Ziolo R F and Zhang X X 1996 *Chem. Mater.* **8** 1784
[20] Zroril R, Machala L, Mashlan M and Sharma V 2004 *Cryst. Growth Des.* **4** 1317
[21] Kodama R H and Berkowitz A E 1998 *Phys. Rev.* B **59** 6321
[22] Khanh B T H L, Hoang V V and Zung H 2008 *Eur. Phys. J.* D **49** 325
[23] Belashchenko D K 1997 *Russ. Chem. Rev.* **66** 733
[24] Signorini L, Pasquini L, Savini L, Carboni R, Boscherini F, Bonetti E, Giglia A, Pedio M, Mahne N and Nannarone S 2003 *Phys. Rev.* B **68** 195423
[25] Roder A, Kob W and Binder K 2001 *J. Chem. Phys.* **114** 7602
[26] Huang J and Bartell L S 2001 *J. Mol. Struct.* **567** 145
[27] Adiga S P, Zapol P and Curtiss L A 2006 *Phys. Rev.* B **74** 064204
[28] George M, Nair S S, Malini K A, Loy P A and Anantharaman M R 2007 *J. Phys. D: Appl. Phys.* **40** 1593
[29] Shimizu K, Brown G M, Habazaki H, Kobayashi K, Skeldon P, Thompson G E and Wood G C 1999 *Corros. Sci.* **41** 1783
[30] Shimizu K, Brown G M, Kobayashi K, Skeldon P, Thompson G E and Wood G C 1998 *Corros. Sci.* **40** 1049
[31] Habazaki H, Shimizu K, Skeldon P, Thompson G E, Wood G C and Zhou X 1997 *Corros. Sci.* **39** 731
[32] Hoang V V, Zung H and Trong N H B 2007 *Eur. Phys. J.* D **44** 515
[33] Hoang V V 2008 *Nanotechnology* **19** 105706
[34] Hoang V V 2007 *J. Phys. Chem.* B **111** 12649
[35] Hoang V V 2007 *J. Phys. D: Appl. Phys.* **40** 7454
[36] Hoang V V and Zung H 2007 Amorphous–amorphous phase transition in amorphous simulated SiO_2 nanoparticles *Tech. Proc. 2007 NSTI Nanotechnology Conf. and Trade Show (Santa Clara, CA, USA, May)*
[37] Hoang V V and Odagaki T 2008 *Phys. Rev.* B **77** 125434
Hoang V V and Odagaki T 2008 *Phil. Mag.* **88** 1461
[38] Hoang V V, Tuan Anh N H and Zung H 2008 *Phys. Status Solidi* b **245** 1505
[39] Rajh T, Nedeljkovic J M, Chen L X, Poluektov O and Thurnauer M C 1999 *J. Phys. Chem.* B **103** 3515
[40] Morales M P, Serna C J, Bodker F and Morup S 1997 *J. Phys.: Condens. Matter* **9** 5461
[41] Ferreira A A L, Abrantes J C C, Jurado J R and Frade J R 2000 *Solids State Ion.* **135** 761
[42] Zhang H and Banfield J F 1998 *J. Mater. Chem.* **8** 20173
[43] Mazurin O V, Streltsina M V and Shvaiko-Shvaikovskaya T P 1983 *Handbook of Glass Data* (Amsterdam: Elsevier)
[44] Baetzold R C and Yang H 2003 *J. Phys. Chem.* B **107** 14357
[45] Preisinger M, Krispin M, Rudolf T, Horn S and Strongin D R 2005 *Phys. Rev.* B **71** 165409
[46] Vollmayr K, Kob W and Binder K 1996 *Phys. Rev.* B **54** 15808
[47] Hoang V V 2007 *Phys. Rev.* B **75** 174202

[48] Hoang V V and Linh N N 2007 *J. Phys. Soc. Japan* **76** 114602
[49] Zhang Z, Zhao M and Jiang Q 2001 *Physica* B **293** 232
[50] Xia Y, Dosseh G, Morineau D and Alba-Simionesco C 2006 *J. Phys. Chem.* B **110** 19735
[51] Jackson C L and McKenna G B 1991 *J. Non-Cryst. Solids* **131–133** 221
[52] Zhang J, Liu G and Jonas J 1992 *J. Phys. Chem.* **96** 3478
[53] Alcoutlabi M and McKenna G B 2005 *J. Phys.: Condens. Matter* **17** R461
[54] Wang X and Zhou W 2002 *Macromolecules* **35** 6747
[55] Schuller J, Melnichenko Y B, Richert R and Fischer E W 1994 *Phys. Rev. Lett.* **73** 2224
[56] Jackson C L and McKenna G B 1996 *Chem. Mater.* **8** 2128
[57] Jiang Q, Shi H S and Zhao M 1999 *J. Chem. Phys.* **111** 2175
[58] McCoy J D and Curro J G 2002 *J. Chem. Phys.* **116** 9154